

# Anisotropic magnetic excitations of a frustrated bilinear-biquadratic spin model – Implications for spin waves of detwinned iron pnictides

Changle Liu,<sup>1</sup> Xingye Lu,<sup>2</sup> Pengcheng Dai,<sup>3</sup> Rong Yu,<sup>4,\*</sup> and Qimiao Si<sup>3,†</sup>

<sup>1</sup>*State Key Laboratory of Surface Physics and Department of Physics, Fudan University, Shanghai, 200433, China*

<sup>2</sup>*Center for Advanced Quantum Studies and Department of Physics, Beijing Normal University, Beijing 100875, China*

<sup>3</sup>*Department of Physics & Astronomy, Rice Center for Quantum Materials, Rice University, Houston, Texas 77005, USA*

<sup>4</sup>*Department of Physics and Beijing Key Laboratory of Opto-electronic Functional Materials and Micro-nano Devices, Renmin University of China, Beijing 100872, China*

(Dated: February 19, 2024)

Elucidating the nature of spin excitations is important to understanding the mechanism of superconductivity in the iron pnictides. Motivated by recent inelastic neutron scattering measurements in the nearly 100% detwinned  $\text{BaFe}_2\text{As}_2$ , we study the spin dynamics of an  $S = 1$  frustrated bilinear-biquadratic Heisenberg model in the antiferromagnetic phase with wavevector  $(\pi, 0)$ . The biquadratic interactions are treated in a dynamical way using a flavor-wave theory in an  $SU(3)$  representation. Besides the dipolar spin wave (magnon) excitations, the biquadratic interactions give rise to quadrupolar excitations at high energies. We find that the quadrupolar wave significantly influences, in an energy dependent way, the anisotropy between the spin excitation spectra along the  $(\pi, 0)$  and  $(0, \pi)$  directions in the wave vector space. Our theoretical results capture the essential behavior of the spin dynamics measured in the antiferromagnetic phase of the detwinned  $\text{BaFe}_2\text{As}_2$ . More generally, our results underscore the importance of electron correlation effects for the microscopic physics of the iron pnictides.

## I. INTRODUCTION

In iron pnictides, superconductivity develops near an antiferromagnetic order in the temperature-doping phase diagram. It is therefore believed that understanding the nature of magnetic excitations is crucial for uncovering the mechanism of superconductivity in these materials.<sup>1–6</sup> The iron pnictides are bad metals. Their room temperature resistivity, about 0.4 m $\Omega$ -cm, is larger than the Mott-Ioffe-Regel limit<sup>2</sup>. This implicates strong electron-electron scatterings that are associated with the underlying electron correlations. In addition, the optical conductivity reveals a large reduction of the Drude weight<sup>7</sup>, signifying a small coherent electron spectral weight  $w$ ; correspondingly, the incoherent electron spectral weight  $(1 - w)$  is larger than the coherent electron counterpart. To the zeroth order in  $w$ , the system is located at the Mott transition; the entire single-electron excitations are incoherent and they give rise to quasi-localized magnetic moments<sup>8</sup>. The coherent itinerant electrons with weight  $w$  will influence the spin excitation spectrum at the linear and higher orders in  $w$ .<sup>8–10</sup> The interactions between the local moments include the  $J_1$ - $J_2$  Heisenberg interactions. Moreover, in the regime near the Mott transition, the multiorbital nature of the underlying electronic system implies that interactions involving multiple spin operators such as the biquadratic  $K$  coupling naturally arise and can be sizeable<sup>11</sup>. A number of additional perspectives have been taken to consider the electron correlation effects<sup>12–37</sup>.

The parent 122 iron pnictides, such as  $\text{BaFe}_2\text{As}_2$ , exhibit a  $(\pi, 0)$  antiferromagnetic (AFM) order at low temperatures.<sup>4</sup> Right at or slightly above the magnetic ordering temperature  $T_N$ , a tetragonal-to-orthorhombic

structural transition takes place, breaking the  $C_4$  spatial rotational symmetry. As a consequence, the low-temperature spin excitations are anisotropic in the wave vector space<sup>38–46</sup>, with equal-energy intensity distribution forming ellipses that are centered around the wave vector  $(\pi, 0)$  at low energies.<sup>43,44</sup> With increasing energy, the elliptic feature expands and the spectral weights transfer from  $(\pi, 0)$  to  $(\pi, \pi)$  of the Brillouin zone (BZ).<sup>44,45</sup>

These properties are well understood by an effective  $S = 1$  bilinear-biquadratic Heisenberg model, for the quasi-localized magnetic moments that are produced by electron correlations in bad metals such as the iron pnictides.<sup>22,30–32</sup> The Hamiltonian of this model reads as follows:

$$H = \frac{1}{2} \sum_{ij} \{ J_{ij} \mathbf{S}_i \cdot \mathbf{S}_j - K_{ij} (\mathbf{S}_i \cdot \mathbf{S}_j)^2 \} \quad (1)$$

where  $J_{ij} = J_1$  and  $K_{ij} = K_1$  are exchange couplings for the nearest neighbor (NN) bonds on a square lattice, and  $J_{ij} = J_2$  and  $K_{ij} = K_2$  are for the next nearest neighbor (NNN) bonds. In the remainder of this manuscript, we refer to the above model as the  $J$ - $K$  model.

Because the biquadratic term involves higher order spin interactions, it is difficult to be handled within any conventional spin-wave theory. For the iron pnictides, the spin dynamics in its  $(\pi, 0)$  AFM phase was thought to be described in terms of an empirical  $J_{1a}$ - $J_{1b}$ - $J_2$  model<sup>38,47</sup>, where  $J_{1a}$  and  $J_{1b}$  refer to the nearest-neighbor  $J_1$  interactions along the tetragonal  $a$  and  $b$  axes, respectively. This effective description would arise from the  $J$ - $K$  model if one makes a *static* approximation to the biquadratic interactions<sup>22</sup>, with the biquadratic interaction being decomposed via a Hubbard-Stratonovich field

( $\Gamma_{ij} = \langle \mathbf{S}_i \cdot \mathbf{S}_j \rangle$ ) that is determined self-consistently. However, the  $J$ - $K$  model is more fundamental than the  $J_{1a}$ - $J_{1b}$ - $J_2$  model. In contrast to the latter, the  $J$ - $K$  model respects the underlying tetragonal lattice symmetry. For example, the  $J$ - $K$  model is able to describe the spin excitation spectrum in the paramagnetic phase, in which  $J_{1a} = J_{1b}$  is dictated by the tetragonal symmetry<sup>22</sup>. It is worth noting that the  $J$ - $K$  model has a very rich ground-state phase diagram. In addition to the  $(\pi, 0)$  AFM order discussed here, it contains ground states that explain the various emergent nematicity in iron-based superconductors, such as in the bulk FeSe and heavily hole-doped iron pnictides<sup>28,37</sup>.

Recent inelastic neutron scattering (INS) measurements on almost fully detwinned  $\text{BaFe}_2\text{As}_2$  samples<sup>48</sup> provide new clues to the nature of the spin excitations in these compounds. Though the measured magnon dispersion in the AFM phase can be well understood by the  $J_{1a}$ - $J_{1b}$ - $J_2$  Heisenberg model up to about 100 meV, the anisotropy of the spectral weights between  $(\pi, 0)$  and  $(0, \pi)$  in the Brillouin zone (BZ) can not. It shows a strong energy dependence and, contrary to the expectation of the  $J_{1a}$ - $J_{1b}$ - $J_2$  model, the observed local (*i.e.*,  $\mathbf{q}$ -integrated) spectral weights near  $(\pi, 0)$  and  $(0, \pi)$  approach each other at high energies.<sup>48</sup>

Here we show that the seemingly unusual spin excitation anisotropy can be naturally understood in terms of the dynamics induced by the biquadratic interaction. We start from the intuitive picture that the high-energy spin excitations correspond to short-range and short-time fluctuations, whose spatial profile will be similar to that of the paramagnetic phase; in the latter case, the spin excitations of the  $J$ - $K$  model will be  $C_4$  symmetric, which is to be contrasted with those of the  $J_{1a}$ - $J_{1b}$ - $J_2$  model that are inherently anisotropic. With this picture in mind, we will analyze the biquadratic  $K$  interaction of the  $S = 1$   $J$ - $K$  model *dynamically*. The ensuing quadrupolar excitations at high energies contribute to a spin excitation spectrum with a considerably reduced anisotropy. We calculate the dynamical spin susceptibilities from the microscopic model, with results that semi-quantitatively account for the puzzling neutron scattering results of the detwinned  $\text{BaFe}_2\text{As}_2$ .

More specifically, we analyze the model, Eq. (1), in terms of an  $SU(3)$  flavor-wave theory. The  $SU(3)$  representation<sup>49</sup>, which treats the  $J$  and  $K$  terms on an equal footing, has previously been used in studying the spin dynamics of iron-based superconductors<sup>28,30</sup>. In the AFM ground state, it incorporates the quadrupolar excitations along with the magnetic dipolar (magnon) ones. While single quadrupolar excitations are orthogonal to the dipolar channel, their convolution with the magnon excitations, for instance, does contribute to the dipolar channel and, hence, to the dynamical spin susceptibility. In this way, the high-energy quadrupolar excitations significantly reduce the anisotropy of the high-energy spin excitation spectrum; we find that the  $J$ - $K$  model provides an excellent understanding of the inelastic neutron

scattering experiments in the detwinned  $\text{BaFe}_2\text{As}_2$ ,<sup>48</sup> on both the spin excitation anisotropy and *the spin spectral weights*.

We stress that, how to theoretically describe the spin excitations in iron-based superconductors is an outstanding question of the field. The new experiments<sup>48</sup> on the spin excitation anisotropy in the detwinned  $\text{BaFe}_2\text{As}_2$  are particularly significant because they access the entire magnetic band<sup>44</sup>. Our analysis of this new experiment allowed us to extract the effect of quadrupolar excitations in this canonical iron-pnictide system. For the iron chalcogenide FeSe, the role of antiferroquadrupolar channel had already been emphasized<sup>28</sup>. In this sense, our work represents not only an advance for the description of the iron pnictides but also a new way of unifying the overall understandings of both the iron pnictides and iron chalcogenides.

The remainder of the paper is organized as follows. In Sec. II, we introduce the  $SU(3)$  representation for the  $S = 1$   $J$ - $K$  model and describe the calculation of the spin excitation spectrum within the  $SU(3)$  flavor-wave theory<sup>28,30</sup>. We then present our main results, in Sec. III, on the magnetic excitations of the  $J$ - $K$  model. We show how the quadrupolar wave affects the anisotropy of the spin excitation spectrum at high energies, and discuss in detail the frequency dependence of the spin spectral weights. Both are shown to describe well the inelastic neutron scattering measurements in the AFM phase of the detwinned  $\text{BaFe}_2\text{As}_2$ . In Sec. IV, we contrast our results with those of weak-coupling analyses, describe the underestimation of the spin spectral weights in an RPA calculation and discuss its implications, before concluding the paper in Sec. V.

## II. MODEL AND METHOD

We start from the  $S = 1$   $J$ - $K$  model defined in Eq. (1). For  $\text{BaFe}_2\text{As}_2$ , the ground-state magnetic structure is a  $\mathbf{Q} = (\pi, 0)$  collinear AFM order. We assume that the corresponding classical spin configuration of this ordered state has all spins aligned in parallel along the  $S^z$  direction *in the spin space*. To simplify the calculation of the spin excitations, we first perform a site-dependent spin rotation about the  $y$ -axis in the spin space:

$$\tilde{\mathbf{S}}_i = \hat{R}_y(\mathbf{Q} \cdot \mathbf{R}_i) \mathbf{S}_i. \quad (2)$$

After this rotation, the spins in even columns stay unchanged while those in odd columns are rotated by a  $\pi$  angle about the  $y$  axis. Therefore, in the rotated configuration, all spins align ferromagnetically along the (negative)  $\tilde{S}^z$  direction, and the Hamiltonian in the rotated basis keeps translational symmetry. We introduce the  $SU(3)$  flavor-wave representation for the (rotated) spin operators. This is formally done by rewriting the spin

operators in terms of three flavor boson operators<sup>28,30</sup>:

$$\tilde{S}_i^+ = \sqrt{2}(b_{i1}^\dagger b_{i0} + b_{i0}^\dagger b_{i\bar{1}}), \quad (3)$$

$$\tilde{S}_i^- = \sqrt{2}(b_{i\bar{1}}^\dagger b_{i0} + b_{i0}^\dagger b_{i1}), \quad (4)$$

$$\tilde{S}_i^z = b_{i1}^\dagger b_{i1} - b_{i\bar{1}}^\dagger b_{i\bar{1}}, \quad (5)$$

where  $b_{i\alpha}^\dagger$  ( $\alpha = 1, 0, \bar{1}$ ) creates a boson of flavor  $\alpha$  on site  $i$ . The Hilbert space of the bosons is larger than the original spin Hilbert space and includes unphysical states. To limit the boson Hilbert space to its physical sector, a hard constraint is imposed on each site

$$b_{i1}^\dagger b_{i1} + b_{i0}^\dagger b_{i0} + b_{i\bar{1}}^\dagger b_{i\bar{1}} = 1. \quad (6)$$

The magnetic ground state in the rotated spin space is polarized. In the bosonic representation this corresponds to condensation of the  $b_{\bar{1}}$  boson on each site, with the condensate amplitude  $\langle b_{i\bar{1}} \rangle$ . Note that the condensation in the bosonic representation depends on the ground state property in the spin representation. For example, for a quadrupolar ordered state that preserves time-reversal symmetry, the condensation takes place in  $b_x = (b_1 + b_{\bar{1}})/\sqrt{2}$ .

With the  $b_{\bar{1}}$  boson being condensed in the AFM ground state, we turn the constraint in Eq. (6) into the following:

$$b_{i\bar{1}} \approx \sqrt{1 - b_{i1}^\dagger b_{i1} - b_{i0}^\dagger b_{i0}}. \quad (7)$$

Deep in the AFM phase  $b_{i\bar{1}} \sim O(1)$  and we can treat  $b_{i0}$  and  $b_{i1}$  as perturbations. Rewriting the spin Hamiltonian of Eq. (1) in terms of the flavor bosons using Eqs. (3)-(5), and expanding it in terms of  $b_{i0}$  and  $b_{i1}$  up to the quadratic order using Eq. (7), we obtain

$$H \approx H_2 = \frac{1}{2} \sum_{\mathbf{k}} \sum_{\nu=0,1} \left[ A_{\mathbf{k}\nu} (b_{\mathbf{k}\nu}^\dagger b_{\mathbf{k}\nu} + b_{-\mathbf{k}\nu}^\dagger b_{-\mathbf{k}\nu}) + B_{\mathbf{k}\nu} (b_{\mathbf{k}\nu}^\dagger b_{-\mathbf{k}\nu}^\dagger + b_{\mathbf{k}\nu} b_{-\mathbf{k}\nu}) \right], \quad (8)$$

where

$$A_{\mathbf{k}0} = 2J_1 \cos k_y + 2K_1 + 4(J_2 + K_2), \quad (9)$$

$$B_{\mathbf{k}0} = -2(J_1 + K_1) \cos k_x - 4(J_2 + K_2) \cos k_x \cos k_y, \quad (10)$$

$$A_{\mathbf{k}1} = 8J_2 - 2K_1 \cos k_y + 4K_2, \quad (11)$$

$$B_{\mathbf{k}1} = -2K_1 \cos k_x - 4K_2 \cos k_x \cos k_y. \quad (12)$$

With the  $b_{\bar{1}}$  boson condensed,  $b_0^\dagger$  corresponds to creating a magnon (spin-1 dipolar excitation) that increases the spin angular momentum  $\tilde{S}^z$  by 1, whereas  $b_1^\dagger$  corresponds to creating spin-2 quadrupolar excitation that increases  $\tilde{S}^z$  by 2. The dipolar and quadrupolar operators do not mix at the quadratic order because they respectively carry spin-1 and spin-2 angular momenta (and, in addition, they possess different parities<sup>50</sup>).

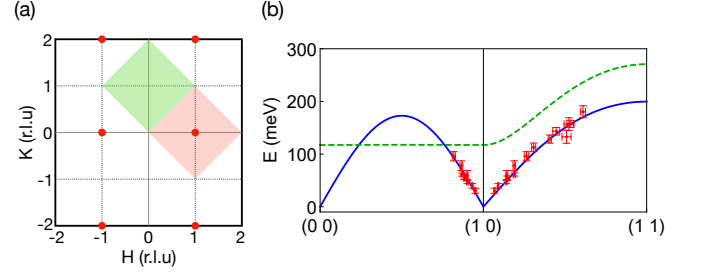


FIG. 1. (a): Reciprocal space of the detwinned BaFe<sub>2</sub>As<sub>2</sub> in the  $(\pi, 0)$  AFM phase. The magnetic Bragg peak positions of the  $(\pi, 0)$  magnetic order are marked as red dots. The integrated areas centered at  $(\pi, 0)$  and  $(0, \pi)$  in Eq. (22) are shown by red and green diamonds, respectively. (b): Dispersions of the bilinear-biquadratic model from the  $SU(3)$  flavor-wave theory. See text for the model parameters. The dots with error bars show the measured dispersion data of a detwinned BaFe<sub>2</sub>As<sub>2</sub> at  $T = 7$  K, extracted from Ref. 48.

The quadratic Hamiltonian in Eq. (8) can be diagonalized via a Bogoliubov transformation

$$b_{\mathbf{k}\nu} = u_{\mathbf{k}\nu} \beta_{\mathbf{k}\nu} + v_{\mathbf{k}\nu} \beta_{-\mathbf{k}\nu}^\dagger \quad (13)$$

where

$$u_{\mathbf{k}\nu} = \sqrt{\frac{A_{\mathbf{k}\nu} + \omega_{\mathbf{k}\nu}}{2\omega_{\mathbf{k}\nu}}}, \quad (14)$$

$$v_{\mathbf{k}\nu} = -\text{sgn}(B_{\mathbf{k}\nu}) \sqrt{\frac{A_{\mathbf{k}\nu} - \omega_{\mathbf{k}\nu}}{2\omega_{\mathbf{k}\nu}}}, \quad (15)$$

$$\omega_{\mathbf{k}\nu} = \sqrt{A_{\mathbf{k}\nu}^2 - B_{\mathbf{k}\nu}^2}. \quad (16)$$

The diagonalized Hamiltonian reads

$$H_2 = \sum_{\mathbf{k}} \sum_{\nu=0,1} \omega_{\mathbf{k}\nu} \beta_{\mathbf{k}\nu}^\dagger \beta_{\mathbf{k}\nu} + C, \quad (17)$$

where  $C$  refers to the zero point energy of the AFM ordered state, and  $\beta_{\mathbf{k}0}$  and  $\beta_{\mathbf{k}1}$  terms describe the excitations of dipolar spin waves (magnons) and quadrupolar waves, respectively.

With the diagonalized Hamiltonian we can readily calculate the dynamical structure factor (DSF) of spins, which is defined as

$$\mathcal{S}(\mathbf{q}, \omega) = \int_{-\infty}^{\infty} \frac{dt}{2\pi} e^{i\omega t} \langle \mathbf{S}_{\mathbf{q}}(t) \cdot \mathbf{S}_{-\mathbf{q}}(0) \rangle, \quad (18)$$

where  $\mathbf{S}_{\mathbf{q}} = \frac{1}{\sqrt{N}} \sum_{\mathbf{k}} \mathbf{S}_i e^{i\mathbf{R}_i \cdot \mathbf{q}}$  is the Fourier transformed spin component.

In the  $SU(3)$  flavor-wave theory the DSF can be separated into two parts,  $\mathcal{S}(\mathbf{q}, \omega) = \mathcal{S}_c(\mathbf{q}, \omega) + \mathcal{S}_i(\mathbf{q}, \omega)$ . The coherent part  $\mathcal{S}_c(\mathbf{q}, \omega)$  comes from one-magnon process

$$\mathcal{S}_c(\mathbf{q}, \omega) = (u_{\mathbf{q}0} - v_{\mathbf{q}0})^2 \delta(\omega - \omega_{\mathbf{q}0}), \quad (19)$$

whereas the incoherent part  $\mathcal{S}_i(\mathbf{q}, \omega)$  contains various two-particle contributions.

$$\begin{aligned} \mathcal{S}_i(\mathbf{q}, \omega) &= \frac{1}{N} \sum_{\mathbf{k}, \mathbf{k}'=\mathbf{q}-\mathbf{k}} \left[ (v_{\mathbf{k}0}u_{\mathbf{k}'1} - u_{\mathbf{k}0}v_{\mathbf{k}'1})^2 \delta(\omega - \omega_{\mathbf{k}1} - \omega_{\mathbf{k}'0}) \right. \\ &+ 2(v_{\mathbf{k}1}v_{\mathbf{k}'1} - v_{\mathbf{k}1}u_{\mathbf{k}'1})^2 \delta(\omega - \omega_{\mathbf{k}1} - \omega_{\mathbf{k}'1}) \\ &\left. + \frac{1}{2}(u_{\mathbf{k}0}v_{\mathbf{k}'0} - v_{\mathbf{k}0}u_{\mathbf{k}'0})^2 \delta(\omega - \omega_{\mathbf{k}0} - \omega_{\mathbf{k}'0}) \right]. \end{aligned} \quad (20)$$

where the three terms from top to bottom on the right hand side correspond to contributions from magnon-quadrupole, two-quadrupole, and two-magnon processes, respectively<sup>30</sup>.

### III. SPIN EXCITATION SPECTRUM

#### A. Magnon and quadrupolar-wave dispersions

To understand the spin excitations in iron pnictides we start by calculating the spin-wave (magnon) and quadrupolar-wave dispersions in the  $J$ - $K$  model from Eqs. (8)-(17). The result is shown in Fig. 1. The model parameters used in this plot are  $J_1 = -9.2 \pm 1.2$  meV,  $J_2 = 50.0 \pm 5.0$  meV,  $K_1 = 68.4 \pm 3.2$  meV, and  $K_2 = -36.4 \pm 5.0$  meV. They allow for a good fit to the experimentally observed magnon dispersion and, as we see below, define a model whose solution provides a semi-quantitative understanding of the experimentally measured dynamical spin susceptibility. In Fig. 1, the solid line shows the magnon dispersion  $\omega_{\mathbf{k}0}$ . It clearly characterizes the Goldstone mode near  $(\pi, 0)$  and a flat band top near  $(\pi, \pi)$ . The dispersion agrees well with that measured in the detwinned  $\text{BaFe}_2\text{As}_2$ , which is described by the symbols in the figure<sup>44,48</sup>. In addition to the magnon branch, there is a quadrupolar-wave branch in the  $SU(3)$  representation, whose dispersion is shown as the dashed line in Fig. 1. The quadrupolar excitation carries spin angular momentum 2, and can be viewed as a two-magnon bound state. As such, it is generically gapped in an AFM ordered phase. As shown in Fig. 1, for  $\text{BaFe}_2\text{As}_2$  the quadrupolar-wave excitation gap is about 100 meV. We then expect it to primarily influence the spin excitation spectrum at energies  $\gtrsim 100$  meV. This is the reason why the spectrum below about 100 meV (where the magnon dispersion can be probed) can be well understood by the spin-wave theory in the conventional  $SU(2)$  representation<sup>22</sup>.

As seen in Eq. (19), the quadrupolar excitations cannot be directly detected by inelastic neutron measurements since quadrupoles carry spin-2 that do not directly couple to neutrons; the coherent part is only contributed by the one-magnon process. However, two quadrupoles can form an effective spin-1 object that transforms as a magnetic dipole moment under  $SU(2)$  spin rotation operation; correspondingly, the two-quadrupole processes do contribute

to the dynamical spin susceptibility. From similar considerations, the same applies to the one-quadrupole-one-magnon processes. Therefore, quadrupole excitations are manifested as the incoherent continuum of the spin excitation spectrum and are expected to appear at high energies in the inelastic neutron scattering spectrum.

#### B. Dynamical structure factor

We have calculated the spin DSF of the  $J$ - $K$  model using Eqs. (18)-(20) within the  $SU(3)$  flavor-wave theory. The coupling of the quasi-localized magnetic moments with coherent electrons will produce nonzero damping rates<sup>22,31</sup>, which will broaden the  $\delta$  functions into a damped harmonic oscillator profile<sup>44</sup>,

$$\delta(\omega - \omega_{\mathbf{q}0}) \sim \frac{4}{\pi} \frac{\Gamma_{\mathbf{q}} \omega \omega_{\mathbf{q}0}}{(\omega^2 - \omega_{\mathbf{q}0}^2)^2 + 4(\Gamma_{\mathbf{q}} \omega)^2}, \quad (21)$$

where  $\Gamma_{\mathbf{q}} = \Gamma_0 + A \cos^2 \frac{q_x}{2} + B \cos^2 \frac{q_y}{2}$ . The damping parameters are taken from Ref. 44.

We show the constant energy cuts of the calculated DSF at several excitation energies in Fig. 2(a)-(d). At low energies, the peaks of DSF form an ellipse centered at  $(\pi, 0)$  in the first BZ. This is consistent with the  $(\pi, 0)$  AFM ground state of the system, above which the low-energy excitations are the Goldstone modes around the ordering wave vector  $(\pi, 0)$ . By contrast, the spin excitations around  $(0, \pi)$  are gapped, reflecting the broken  $C_4$  symmetry of the ground state. With increasing energy the ellipse centered at  $(\pi, 0)$  expands as shown in Fig. 2(a) and (b). Further increasing the energy above 100 meV, going along the ellipse the spectral weight in the  $q_x$  direction largely decreases and the maximum of the spectral weight is distributed at the long-axis ( $q_y$ ) direction. The ellipse then effectively splits into two parts and the spectral weights transfer along the  $q_y$  direction towards to  $(\pi, \pi)$ , as shown in Fig. 2(c) and (d). These results capture the main features of the measured DSF of detwinned  $\text{BaFe}_2\text{As}_2$  in the corresponding energies shown in Fig. 2(e)-(h).<sup>48</sup>

The DSF calculated from the  $SU(3)$  flavor-wave theory also shows some interesting characteristics that are not captured by the conventional spin-wave theory. In particular, the spectral weights close to  $(\pi, 0)$  and  $(0, \pi)$  are very different at low energies, but this anisotropy is reduced with increasing energy. To see this clearly we calculate the local dynamical susceptibilities  $\chi''_{\mathbf{Q}_i}(\omega)$  over the wave vector regimes near  $\mathbf{Q}_1 = (\pi, 0)$  and  $\mathbf{Q}_2 = (0, \pi)$ , respectively,

$$\chi''_{\mathbf{Q}_{1(2)}}(\omega) = \frac{\int_{\mathbf{q} \in \text{BZ}_{\mathbf{Q}_{1(2)}}} d\mathbf{q} \chi''_{\mathbf{q}}(\omega)}{\int_{\mathbf{q} \in \text{BZ}_{\mathbf{Q}_{1(2)}}} d\mathbf{q}}. \quad (22)$$

where the integration regime  $\text{BZ}_{\mathbf{Q}_{1(2)}}$  is shown in Fig. 1(a), as red and green diamonds respectively. An

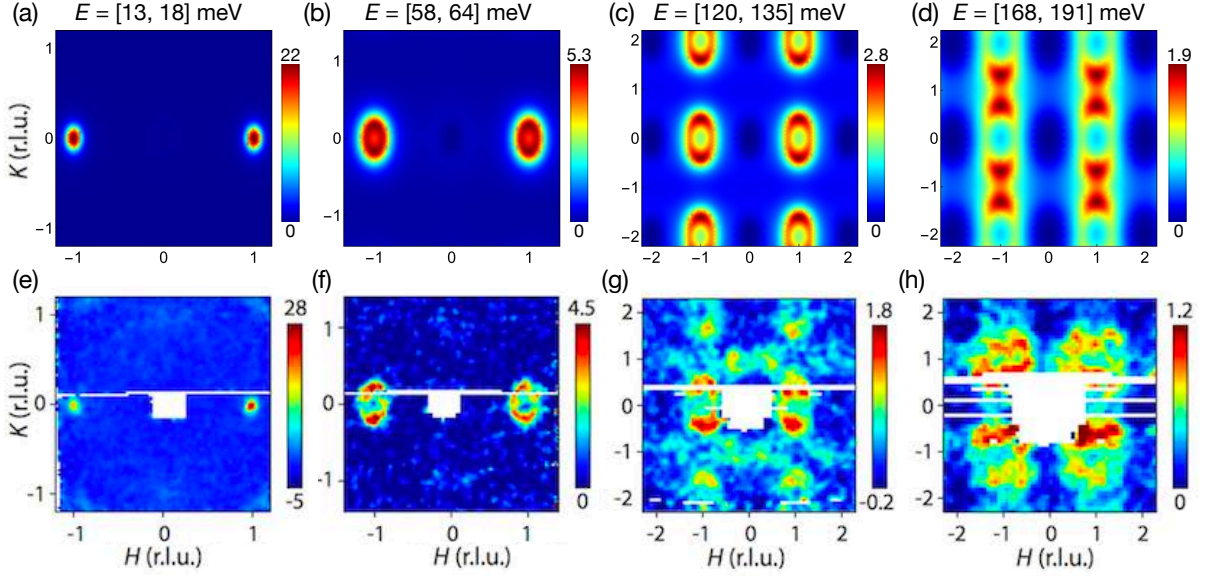


FIG. 2. Constant energy cuts of the magnetic excitation spectrum in the wave vector space for the  $(\pi,0)$  AFM phase of the  $J$ - $K$  model [in (a)-(d)]. For comparison, the corresponding experimental results are shown in (e)-(h). The experimental plots are reproduced from Ref. 48.

anisotropy factor is defined as

$$\Psi(\omega) = \frac{\chi''_{\mathbf{Q}_1}(\omega) - \chi''_{\mathbf{Q}_2}(\omega)}{\chi''_{\mathbf{Q}_1}(\omega) + \chi''_{\mathbf{Q}_2}(\omega)}. \quad (23)$$

The energy dependence of the local susceptibilities and the anisotropy factor  $\Psi$  are shown in Fig. 3. Both local susceptibilities develop broad peaks in between 150 and 200 meV, and exhibit considerable spectral weights up to 300 meV. A major contribution to the high-energy spectral weights comes from the incoherent part of the DSF. The difference between the two local susceptibilities is reduced with increasing energy, and this is clearly seen from the decreasing anisotropy factor  $\Psi$  with increasing energy, as shown in Fig. 3(b). Such a strong energy-dependent spectral weight anisotropy is also observed in the neutron scattering experiment, and our theoretical results agree well with the experimental data. However, as shown in Fig. 3(b), this feature is not captured by the effective  $J_{1a}$ - $J_{1b}$ - $J_2$  model, in which the anisotropy as calculated from the conventional spin-wave theory persists to high energies owing to its intrinsic anisotropic nature.<sup>48</sup>

To understand this energy-dependent spectral weight anisotropy, we recall that the high-energy spectrum contains or is even dominated by the contribution from incoherent part of the DSF. The latter contains various two-particle processes. For a given set of  $(\mathbf{q}, \omega)$  there can be many two-particle processes satisfying the energy and momentum conservation, as shown by the additional summation over  $\mathbf{k}$  in Eq. (20). Some processes may contribute equally to the local spectral weights near  $(\pi, 0)$  and  $(0, \pi)$  and hence reduce the spectral anisotropy. For example, for a given  $\omega$  the contribution to  $\mathcal{S}_i(\pi, 0)$

may come from quasiparticles with momenta  $(\pi/2, \pi/2)$  and  $(\pi/2, -\pi/2)$ , while the contribution to  $\mathcal{S}_i(0, \pi)$  may come from quasiparticles with momenta  $(\pi/2, \pi/2)$  and  $(-\pi/2, \pi/2)$ . Since  $(\pm\pi/2, \pm\pi/2)$  are equivalent points in the BZ, their contributions to  $\mathcal{S}_i(\pi, 0)$  and  $\mathcal{S}_i(0, \pi)$  are equal. While all the three types of two-particle processes in Eq. (20) in principle contribute to the reduction of spectral anisotropy, the dominant contribution at high energies involves the quadrupolar excitations.

#### IV. DISCUSSIONS

In this work, we have provided a semi-quantitative understanding of the anisotropic spin excitation spectrum observed by inelastic neutron scattering experiments in the detwinned  $\text{BaFe}_2\text{As}_2$ . Treating the correlation-induced incoherent electronic excitations in terms of quasi-local moments, we determined the anisotropic dynamical spin susceptibilities of the spin  $S = 1$   $J$ - $K$  model. We did so by analyzing the biquadratic  $K$  interaction dynamically, based on an  $SU(3)$  representation of the spin. Our results, for both the momentum distribution of the dynamical spin susceptibility and the spin excitation anisotropy factor  $\Psi$ , are consistent with the experimental results measured in the detwinned  $\text{BaFe}_2\text{As}_2$ .<sup>48</sup>

The experimental results have alternatively been analyzed in terms of electron-hole excitations within a modified random-phase approximation (RPA) calculation<sup>48</sup>. Weak-coupling approaches, such as RPA calculations, represent an alternative means to realize a  $(\pi, 0)$  AFM phase in the parent iron pnictides.<sup>51–53</sup> Given the relatively small size of the Fermi pockets in these systems,

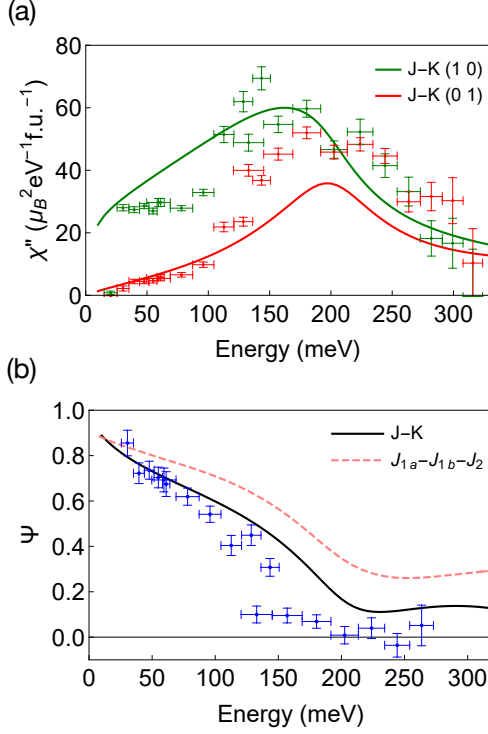


FIG. 3. (a): Comparison of the energy dependence for the local dynamical spin susceptibilities  $\chi_{\mathbf{Q}_{1(2)}}$ , as defined in Eq. 22, with  $\mathbf{Q}_1 = (\pi, 0)$  and  $\mathbf{Q}_2 = (0, \pi)$  respectively marked as (1, 0) and (0, 1), between the experimental data (symbols) and the  $SU(3)$  flavor-wave theory results of the  $J$ - $K$  model (lines). (b): Comparison of the spin excitation anisotropy factor  $\Psi$  between the experimental data (symbols), the  $SU(3)$  flavor-wave results of the  $J$ - $K$  model (black solid curve), and the  $SU(2)$  spin-wave results of the  $J_{1a}-J_{1b}-J_2$  model (pink solid curve). The experimental data for  $\chi_{\mathbf{Q}_{1(2)}}$  in (a) are from Ref. 48, from which the experimental data for  $\Psi$  in (b) are determined according to Eq. (23). The result (pink solid curve) for  $\Psi$  from an  $SU(2)$ -based calculation of the  $J_{1a}-J_{1b}-J_2$  model, shown in (b), is also from Ref. 48.

the standard RPA calculation was known to produce too small a spin spectral weight compared to the experimental measurement. The modified RPA calculation tried to remedy this by introducing a quasiparticle weight  $z < 1$  to mimic the interaction effects. The result of this modified RPA calculation still under-accounts for the experimentally measured dynamical spin susceptibility. This is illustrated in Fig. 4, where we compare the experimental spectral weight data (and our results for the  $J$ - $K$  model) with those from the modified RPA calculation in absolute units. The substantial under-estimation of the spin spectral weight even in the modified RPA calculation points to the dominating contributions from the incoherent electron excitations, which are not captured by such calculations.

In our approach, we account for the spin excitations derived from the incoherent part of the single-electron excitations through quasi-localized magnetic moments and

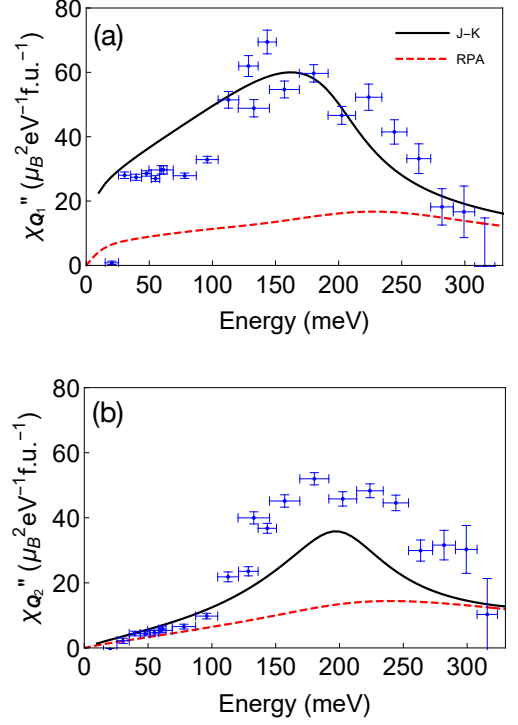


FIG. 4. The energy dependence of the local susceptibilities  $\chi''$ : comparing the experimental data (symbols), the  $SU(3)$  flavor-wave theory of the  $J$ - $K$  model (solid lines), and the modified RPA results (dashed lines) in absolute units. The experimental data and the modified RPA results are from Ref. 48.

describe them in terms of the  $J$ - $K$  model. The semi-quantitative success of our calculations in capturing the experimentally measured spin excitation spectrum reinforces the above conclusion. It suggests that the overall spin dynamics of the iron pnictides in an extended energy range is well described by approaches that are anchored by the fluctuations of local moments. Because the latter describes the spin degrees of freedom produced by the correlation-driven incoherent electronic excitations, our results also imply that the energy scales associated with the anisotropic magnetic fluctuations will be very large as has indeed been observed experimentally (and failed to be described by the modified RPA calculations)<sup>48</sup>. All these aspects underscore the importance of electron correlations in the iron pnictides.

The above considerations reinforce the implications that have been drawn from the presence of Mott insulating phases in both the iron chalcogenide<sup>54–59</sup> and iron pnictide<sup>60</sup> families. An exciting recent development in the same spirit is the observation of magnetic and nematic orders in a semiconducting iron chalcogenide  $\text{KFe}_{0.8}\text{Ag}_{1.2}\text{Te}_2$ ;<sup>61</sup> exploration of the presumably anisotropic spin dynamics in this and related systems promises to shed further light on the role of electron correlations in the overall physics of both the iron pnictides and chalcogenides.



We close this section by noting on several additional points. Firstly, as we alluded to in the introduction, the discrepancy of the observed spin excitation anisotropy with the description by the  $J_{1a}$ - $J_{1b}$ - $J_2$  model is intrinsic and, in particular, is not a reflection of any particular parameter choice. The large  $J_{1a}$ - $J_{1b}$  anisotropy that is needed to understand the spin-wave dispersion inherently implies a large spin excitation anisotropy even for the high energy magnetic excitations at the magnetic zone boundary, in contrast to the experimental observation.

Secondly, and in contrast to the  $J_{1a}$ - $J_{1b}$ - $J_2$  description, the Hamiltonian of the bilinear-biquadratic  $J$ - $K$  model itself respects the tetragonal symmetry. Even with the spontaneous symmetry breaking, in the  $(\pi, 0)$  antiferromagnetic phase, the emergence of quadrupolar excitations hastens the restoration of the tetragonal symmetry at high energies, precisely as the experimental results show. In this sense, the measurement of the high-energy spin excitation anisotropy under the detwinning condition is currently the most direct way of probing the quadrupolar excitations in the iron pnictides.

Our theory implicates a quadrupolar wave excitation existing above 100 meV, though it is hidden to neutron scattering measurements. In principle, the quadrupolar and dipolar moments may mix under a certain magnetic field<sup>62,63</sup>, thereby activating the quadrupolar excitations in magnetic dipolar probes such as neutron scattering experiments. This effect would be significant only when the Zeeman energy of the applied magnetic field is comparable to the typical magnetic energy scale, as happens in heavy fermion systems<sup>64,65</sup>. For the canonical iron pnictide system we discussed, however, the magnetic bandwidth is larger than 100 meV, and the involved exchange coupling is on the order of 10 meV. These energy scales are much larger than that associated with the typical strength of the magnetic field applied in neutron scattering experiments. Hence, within the available experimental capacities, we do not expect the application of an external magnetic field to help resolve the quadrupolar wave excitations more explicitly.

## V. SUMMARY

To summarize, we have investigated the spin excitations of an  $S = 1$  bilinear-biquadratic Heisenberg model

in the antiferromagnetic phase. We find that the magnetic excitations consist of a dipolar spin wave (magnon) at low energies and a quadrupolar wave at high energies. Though the quadrupolar excitations cannot be directly detected by neutron scattering, we show that they can significantly affect the spin excitation spectrum and, in particular, reduce the anisotropy at high energies between the local susceptibilities near  $(\pi, 0)$  and  $(0, \pi)$  in the wave vector space. Our theoretical results capture the essential features of the spin excitations of the detwinned  $\text{BaFe}_2\text{As}_2$ . This suggests that the incoherent part of the single-electron excitations, which give rise to quasilocalized magnetic moments, dominates the contributions to the spin excitations.<sup>9,10</sup> Correspondingly, this implies that electron correlations play a central role in the microscopic physics of the iron-based superconductors.

## ACKNOWLEDGEMENT

We thank the late Elihu Abrahams, Haoyu Hu, Wenjun Hu and Hsin-Hua Lai for useful discussions. This work was supported by the Ministry of Science and Technology of China Grants No. 2016YFA0301001, 2016YFA0300500, and 2018YFGH000095 (C.L.), by the National Natural Science Foundation of China Grant No. 11734002 (X.L.), by the Ministry of Science and Technology of China Grant No. 2016YFA0300504, the National Natural Science Foundation of China Grant No. 11674392, the Fundamental Research Funds for the Central Universities, the Research Funds of Renmin University of China Grant No. 18XNLG24 (R.Y.), and by U. S. NSF DMR-1700081 (P.D.) and by the U.S. Department of Energy, Office of Science, Basic Energy Sciences, under Award No. DE-SC0018197 and the Robert A. Welch Foundation Grant No. C-1411 (Q.S.).

---

\* rong.yu@ruc.edu.cn

† qmsi@rice.edu

<sup>1</sup> Y. Kamihara, T. Watanabe, M. Hirano, and H. Hosono, *J. Am. Chem. Soc.* **130**, 3296 (2008).

<sup>2</sup> D. C. Johnston, *Adv. Phys.* **59**, 803-1061 (2010).

<sup>3</sup> F. Wang and D.-H. Lee, *Science* **332**, 200-204 (2011).

<sup>4</sup> P. Dai, *Rev. Mod. Phys.* **87**, 855-896 (2015).

<sup>5</sup> Q. Si, R. Yu and E. Abrahams, *Nat. Rev. Mater.* **1**, 16017 (2016).

<sup>6</sup> P. J. Hirschfeld, *Comptes Rendus Physique* **17**, 197 (2016).

<sup>7</sup> M. Qazilbash, J. Hamlin, R. Baumbach, L. Zhang, D. J. Singh, M. Maple, and D. Basov, *Nat. Phys.* **5**, 647 (2009).

<sup>8</sup> Q. Si and E. Abrahams, *Phys. Rev. Lett.* **101**, 076401 (2008).

<sup>9</sup> Q. Si, E. Abrahams, J. Dai, and J.-X. Zhu, *New J. Phys.* **11**, 045001 (2009).

<sup>10</sup> J. Dai, Q. Si, J.-X. Zhu, and E. Abrahams, *Proc. Natl. Acad. Sci.* **106**, 4118 (2009).

- <sup>11</sup> P. Fazekas, *Lecture Notes on Electron Correlation and Magnetism* (World Scientific, Singapore, 1999), Chap. 5.
- <sup>12</sup> C. Fang, H. Yao, W.-F. Tsai, J. Hu and S. A. Kivelson Phys. Rev. B **77**, 224509 (2008).
- <sup>13</sup> C. Xu, M. Muller and S. Sachdev, Phys. Rev. B **78**, 020501(R) (2008).
- <sup>14</sup> W.-Q. Chen, K.-Y. Yang, Y. Zhou, and F.-C. Zhang, Phys. Rev. Lett. **102**, 047006 (2009).
- <sup>15</sup> A. Moreo, M. Daghofer, J. A. Riera and E. Dagotto, Phys. Rev. B **79**, 134502 (2009).
- <sup>16</sup> E. Berg, S. A. Kivelson and D. J. Scalapino, New J. Phys. **11**, 085007 (2009).
- <sup>17</sup> F. Ma, Z.-Y. Lu, and T. Xiang, Phys. Rev. B **78**, 224517 (2008).
- <sup>18</sup> M. J. Han, Q. Yin, W. E. Pickett and S. Y. Savrasov, Phys. Rev. Lett. **102** 107003 (2009).
- <sup>19</sup> M. S. Laad, L. Craco, S. Leoni and H. Rosner, Phys. Rev. B **79**, 024515 (2009).
- <sup>20</sup> Z. P. Yin, K. Haule, and G. Kotliar, Nature Mater. **10**, 932 (2011).
- <sup>21</sup> W. Lv, F. Krüger and P. Phillips, Phys. Rev. B **82**, 045125 (2010).
- <sup>22</sup> R. Yu, Z. Wang, P. Goswami, A. H. Nevidomskyy, Q. Si, and E. Abrahams, Phys. Rev. B **86**, 085148 (2012).
- <sup>23</sup> A. L. Wysocki, K. D. Belashchenko and V. P. Antropov, Nat. Phys. **7**, 485 (2011).
- <sup>24</sup> G. S. Uhrig, M. Holt, J. Oitmaa, O. P. Sushkov and R. R. P. Singh, Phys. Rev. B **79**, 092416 (2009).
- <sup>25</sup> H. Ishida and A. Liebsch, Phys. Rev. B **81**, 054513 (2010).
- <sup>26</sup> G. Giavannetti, C. Ortix, M. Marsman, M. Capone, J. van den Brink and J. Lorenzana, Nat. Commun. **2**, 398 (2011).
- <sup>27</sup> M. J. Calderón, F. Le'on, B. Valenzuela and E. Bascones, Phys. Rev. B **86**, 104514 (2012).
- <sup>28</sup> R. Yu and Q. Si, Phys. Rev. Lett. **115**, 116401 (2015).
- <sup>29</sup> F. Wang, S. A. Kivelson, and D.-H. Lee, Nat. Phys. **11**, 959 (2015).
- <sup>30</sup> C. Luo, T. Datta, and D.-X. Yao, Phys. Rev. B **93**, 235148 (2016).
- <sup>31</sup> P. Goswami, R. Yu, Q. Si, and E. Abrahams, Phys. Rev. B **84**, 155108 (2011).
- <sup>32</sup> D. Stanek, O. P. Sushkov, and G. S. Uhrig, Phys. Rev. B **84**, 064505 (2011).
- <sup>33</sup> R. Yu, Q. Si, P. Goswami, and E. Abrahams, J. Phys.: Conf. Ser. **449**, 012025 (2013).
- <sup>34</sup> P. B. Ergueta and A. H. Nevidomskyy, Phys. Rev. B **92**, 165102 (2015).
- <sup>35</sup> H.-H. Lai, W.-J. Hu, E. M. Nica, R. Yu, and Q. Si, Phys. Rev. Lett. **118**, 176401 (2017).
- <sup>36</sup> H. Ruiz, Y. Wang, B. Moritz, A. Baum, R. Hackl, and T. P. Devereaux, Phys. Rev. B **83**, 214519 (2011).
- <sup>37</sup> Y. Wang, W. Hu, R. Yu, and Q. Si, Phys. Rev. B **100**, 100502(R) (2019).
- <sup>38</sup> J. Zhao, D. Adroja, D.-X. Yao, R. Bewley, S. Li, X. Wang, G. Wu, X. Chen, J. Hu, and P. Dai, Nat. Phys. **5**, 555 (2009).
- <sup>39</sup> D. Inosov, J. Park, P. Bourges, D. Sun, Y. Sidis, A. Schneidewind, K. Hradil, D. Haug, C. Lin, B. Keimer, and V. Hinkov, Nat. Phys. **6**, 178 (2010).
- <sup>40</sup> C. Lester, J.-H. Chu, J. G. Analytis, T. G. Perring, I. R. Fisher, and S. M. Hayden, Phys. Rev. B, **81**, 064505 (2010).
- <sup>41</sup> H.-F. Li, C. Broholm, D. Vaknin, R. M. Fernandes, D. L. Abernathy, M. B. Stone, D. K. Pratt, W. Tian, Y. Qiu, N. Ni, S. O. Diallo, J. L. Zarestky, S. L. Bud'ko, P. C. Canfield, and R. J. McQueeney, Phys. Rev. B **82**, 140503 (2010).
- <sup>42</sup> J. T. Park, D. S. Inosov, A. Yaresko, S. Graser, D. L. Sun, P. Bourges, Y. Sidis, Y. Li, J.-H. Kim, D. Haug, A. Ivanov, K. Hradil, A. Schneidewind, P. Link, E. Faulhaber, I. Glavatsky, C. T. Lin, B. Keimer, and V. Hinkov, Phys. Rev. B **82**, 134503 (2010).
- <sup>43</sup> S. O. Diallo, D. K. Pratt, R. M. Fernandes, W. Tian, J. L. Zarestky, M. Lumsden, T. G. Perring, C. L. Broholm, N. Ni, S. L. Bud'ko, P. C. Canfield, H.-F. Li, D. Vaknin, A. Kreyssig, A. I. Goldman, and R. J. McQueeney, Phys. Rev. B **81**, 214407 (2010).
- <sup>44</sup> L. W. Harriger, H. Q. Luo, M. S. Liu, C. Frost, J. P. Hu, M. R. Norman, and Pengcheng Dai, Phys. Rev. B **84**, 054544 (2011).
- <sup>45</sup> R. A. Ewings, T. G. Perring, J. Gillett, S. D. Das, S. E. Sebastian, A. E. Taylor, T. Guidi, and A. T. Boothroyd, Phys. Rev. B **83**, 214519 (2011).
- <sup>46</sup> M. Liu, L. W. Harriger, H. Luo, M. Wang, R. Ewings, T. Guidi, H. Park, K. Haule, G. Kotliar, S. Hayden and P. Dai, Nat. Phys. **8**, 376 (2012).
- <sup>47</sup> R. Applegate, J. Oitmaa, R. R. P. Singh, Phys. Rev. B **81**, 024505 (2010).
- <sup>48</sup> X. Lu, D. D. Scherer, D. W. Tam, W. Zhang, R. Zhang, H. Luo, L. W. Harriger, H. C. Walker, D. T. Adroja, B. M. Andersen, and P. Dai, Phys. Rev. Lett. **121**, 067002 (2018).
- <sup>49</sup> A. Läuchli, F. Mila, and K. Penc, Phys. Rev. Lett. **97**, 087205 (2006).
- <sup>50</sup> The parity is defined by the  $\mathbb{Z}_2$  symmetry of the Hamiltonian generated by  $G \equiv \exp[i\pi \sum_i \tilde{S}_i^z]$ .
- <sup>51</sup> S. Graser, T. Maier, P. Hirschfeld, and D. Scalapino, New J. Phys. **11**, 025016 (2009).
- <sup>52</sup> Y. Ran, F. Wang, H. Zhai, A. Vishwanath, and D.-H. Lee, Phys. Rev. B **79**, 014505 (2009).
- <sup>53</sup> J. Knolle, I. Eremin, A. Chubukov, and R. Moessner, Phys. Rev. B **81**, 140506(R) (2010).
- <sup>54</sup> J.-X. Zhu, R. Yu, H. Wang, L. L. Zhao, M. D. Jones, J. Dai, E. Abrahams, E. Morosan, M. Fang, and Q. Si, Phys. Rev. Lett. **104**, 216405 (2010).
- <sup>55</sup> D. G. Free and J. S. O. Evans, Phys. Rev. B **81**, 214433 (2010).
- <sup>56</sup> B. Freelon, Y. H. Liu, J.-L. Chen, L. Craco, M. S. Laad, S. Leoni, J. Chen, L. Tao, H. Wang, R. Flauca, Z. Yamani, M. Fang, C. Chang, J.-H. Guo, and Z. Hussain, Phys. Rev. B **92**, 155139 (2015).
- <sup>57</sup> M.-H. Fang, H.-D. Wang, C.-H. Dong, Z.-J. Li, C.-M. Feng, J. Chen, and H. Q. Yuan, Euro. Phys. Lett. **94**, 27009 (2011).
- <sup>58</sup> D. M. Wang, J. B. He, T.-L. Xia and G. F. Chen, Phys. Rev. B **83**, 132502 (2011).
- <sup>59</sup> M. Wang, M. Yi, H. Cao, C. de la Cruz, S. K. Mo, Q. Z. Huang, E. Bourret-Courchesne, P. C. Dai, D. H. Lee, Z. X. Shen, and R. J. Birgeneau, Phys. Rev. B **92**, 121101 (2015).
- <sup>60</sup> Y. Song, Z. Yamani, C. Cao, Y. Li, C. Zhang, J. S. Chen, Q. Huang, H. Wu, J. Tao, Y. Zhu, W. Tian, S. Chi, H. Cao, Y.-B. Huang, M. Dantz, T. Schmitt, R. Yu, A. H. Nevidomskyy, E. Morosan, Q. Si and P. Dai, Nature Commun. **7**, 13879 (2016).
- <sup>61</sup> Y. Song, H. Cao, B. C. Chakoumakos, Y. Zhao, A. Wang, H. Lei, C. Petrovic, and R. J. Birgeneau, Phys. Rev. Lett. **122**, 087201 (2019).



- <sup>62</sup> A. Smerald and N. Shannon, Phys. Rev. B **88**, 184430 (2013).
- <sup>63</sup> V. Barzykin and L. P. Gor'kov, Phys. Rev. Lett. **70**, 2479 (1993).
- <sup>64</sup> P. Y. Portnichenko, S. E. Nikitin, A. Prokofiev, S. Paschen, J.-M. Mignot, J. Ollivier, A. Podlesnyak, Siqin Meng, Zhilun Lu, and D. S. Inosov Phys. Rev. B **99**, 214431 (2019).
- <sup>65</sup> J. Custers, K. A. Lorenzer, M. Müller, A. Prokofiev, A. Sidorenko, H. Winkler, A. M. Strydom, Y. Shimura, T. Sakakibara, Rong Yu, Q. Si, and S. Paschen, Nat. Mater. **11**, 189-194 (2012).